



1 **Design of parametric risk transfer solutions for volcanic**
2 **eruptions: an application to Japanese volcanoes**

3 Delioma Oramas-Dorta¹, Giulio Tirabassi¹, Guillermo E. Franco¹, Christina Magill²

4 ¹ Guy Carpenter & Co, LLC. Tower Place West, London, EC3 5BU, United Kingdom.

5 ² Department of Environmental Sciences, Faculty of Science and Engineering, Macquarie University, NSW 2109,
6 Australia.

7 *Correspondence to:* Dr. Delioma Oramas-Dorta (Delioma.Oramas-Dorta@guycarp.com).

8

9

10

11

12

13

14

15

16

17

18

19

20

21

22

23

24

25

26

27



28 **Abstract**

29 Volcanic eruptions are rare but potentially catastrophic phenomena, affecting societies and economies through
30 different pathways. The 2010 Eyjafjallajökull eruption in Iceland, a medium-sized ash fall producing eruption,
31 caused losses in the range of billions of dollars, mainly to the aviation and tourist industries. Financial risk transfer
32 mechanisms such as insurance are used by individuals, companies, Governments, etc. to protect themselves from
33 losses associated to natural catastrophes. In this work, we conceptualize and design a parametric risk transfer
34 mechanism to offset losses to building structures arising from large, ash fall-producing volcanic eruptions. Such
35 transfer mechanism relies on the objective measurement of physical characteristics of volcanic eruptions that are
36 correlated with the size of resulting losses (in this case, height of the eruptive column and predominant direction of
37 ash dispersal), in order to pre-determine payments to the risk cedant concerned. We apply this risk transfer
38 mechanism to the case of Mount Fuji in Japan, by considering a potential risk cedant such as a regional Government
39 interested in offsetting losses to dwellings in the heavily populated Prefectures of Tokyo and Kanagawa. The
40 simplicity in determining eruptive column height and ash fall dispersal direction makes this design suitable for
41 extrapolation to other volcanic settings world-wide where significant ash fall producing eruptions may occur,
42 provided these parameters are reported by an official, reputable agency, and a suitable loss model is available for the
43 volcanoes of interest.

44

45

46

47

48

49

50

51

52

53

54

55

56

57

58

59

60

61



62 1 Introduction

63 Volcanic eruptions are complex phenomena that generate a variety of hazards such as lava flows, ash fall,
64 pyroclastic flows, lahars, and volcanic earthquakes. These may in turn cause physical damage to man-made
65 structures and the discontinuation of activities related to aviation, tourism, and agriculture, among others.

66 Although rare, large volcanic eruptions pose significant destructive and disruptive potential. A medium-sized
67 eruption like the 2010 Eyjafjallajökull eruption in Iceland (VEI¹ 4) caused the cancellation of about one hundred
68 thousand flights and carried an estimated global cost of US\$4.7 Billion (Oxford Economics, 2010). According to
69 estimates by the Government of Japan, a repeat of the December 1707 Mt. Fuji eruption (VEI 5) could result in
70 national losses over US\$22.5 Billion (Cabinet Office of Japan, 2002), not including impacts on transportation and
71 power transmission facilities that could effectively paralyze the Tokyo metropolitan area. Mt. Tambora's 1815
72 eruption in Indonesia (VEI 7) is regarded as the greatest eruption in historic time, ejecting as much as 175 km³ of
73 pyroclastic material that reached heights of over 40 km into the atmosphere (Self et al., 1984). It caused an estimated
74 death toll of 71,000 people some of which due to the immediate explosion that killed around 12,000 people on
75 Sumbawa Island (Oppenheimer, 2003). The event triggered tsunami waves striking several Indonesian islands and a
76 famine related to eruptive fallout ruining crops in the region (Stothers, 1984; Oppenheimer, 2003). At present, over
77 one million people live within 100km of Mt. Tambora (GVP, 2019).

78 Insurance is a mechanism to protect against financial losses from natural perils. Through insurance, people and
79 entities transfer risks to insurance companies in return for the payment of an annual premium. These premiums are
80 accumulated in order to build up reserves that enable them to pay claims in case of need. Insurance companies,
81 similarly, can accept only a certain amount of risk, after which they may themselves seek protection through
82 reinsurance. Companies who sell reinsurance are typically global in nature, hedging their risk in one region by
83 selling products in another or by seeking insurance mechanisms themselves for their own portfolios (this is called
84 "retrocession"). Through this chain of risk transfer accumulations of risk are successfully shared among many
85 parties across the world, ideally enabling our society to cope with potentially large losses without any particular
86 entity in this chain suffering unrecoverable losses.

87
88 As concentrations of risks grew, the capital available to supply global reinsurance products was in more demand,
89 which had the consequence of raising prices. A larger supply of capital was necessary and there were large yields
90 available for those interested. This gave rise to the appearance of Insurance Linked Securities (ILS), a type of
91 financial instrument that allowed the capital markets to enter the insurance space in what has been referred to as "the
92 convergence market," thus increasing the amount of capital available for insurance-related operations. One tool that
93 falls into this category is a catastrophe (cat) bond, a means of fragmenting risk into coupon bonds that can be sold to
94 qualified investors (Cummins, 2008; Swiss Re, 2011).

95
96 As new investors in this space lack familiarity with traditional insurance operations, there has been an interest in
97 devising some of these instruments as a form of derivative that simplifies the process of settling a claim (World
98 Economic Forum, 2008). This motivation gave rise to "parametric cat bonds" in which recoveries after a catastrophe
99 event are tied to the occurrence of a set of measurable physical characteristics, such as the magnitude of an
100 earthquake or the category of a hurricane, rather than to actual losses or indemnity. Properly chosen parameters that
101 are easy to measure transparently and with accuracy can provide parametric cat bonds with a speed of payment
102 unparalleled in the domain of insurance. Progressively, as sensors become more ubiquitous and precise, and as

¹ The Volcanic Explosivity Index (VEI) is a relative measure of the explosiveness of volcanic eruptions devised by Chris Newhall and Stephen Self in 1982. The scale is open-ended with the largest eruptions in history given magnitude 8. The scale is logarithmic from VEI 2 upwards, with each interval on the scale representing a tenfold increase in volume of eruptive products.



103 technology facilitates communication of measurements, parametric insurance mechanisms are becoming more
104 widespread.

105

106 Earthquake parametric cat bond transactions appeared first in 1997 and grew in number throughout the following
107 years, supported by what were then relatively novel techniques to model earthquake risk in the insurance market
108 (Franco, 2014). Since then, these earthquake solutions have taken many forms depending on the parameters chosen
109 for their design and on whether they are binary (pay or no pay) or “index-based” indicating a payment somewhat
110 correlated with the intensity of the event (Wald and Franco, 2016; 2017). A similar development in the field of
111 volcanic risks has not yet taken place. Only one product exists in the market, offered by Sompo Japan Nipponkoa
112 Insurance that provides coverage on a parametric basis for volcanic eruptions. This product is addressed to
113 commercial corporations in Japan at risk of experiencing losses derived from a volcanic eruption (Artemis, 2016).
114 Tailored in particular to the tourism industry, it grants coverage of losses up to US\$10 million from business
115 interruption caused by the onset of a level 3 or above eruption alert as determined by the Japan Meteorological
116 Agency (JMA) (Yamasato et al., 2013).

117

118 The dearth of insurance derivative products linked to physical characteristics of volcanic eruptions may be partly
119 explained by the lack of fully probabilistic volcano loss models, which are a pre-requisite for the design and
120 calibration of these products. In this paper we present a stochastic volcanic risk model for six Japanese volcanoes on
121 which we base the construction of a parametric risk transfer tool. First, in Sect. 2 we describe the components of the
122 risk model; i.e. hazard, vulnerability, exposure, and loss computation. In Sect. 3, we discuss the conceptualization
123 and the mathematical design of a plausible parametric risk transfer tool leveraging physical descriptors of the
124 eruptive events that are both simulated in the risk model as well as reported by public entities during the course of an
125 actual event. The work draws from efforts carried out in the development of parametric triggers for other perils,
126 fundamentally earthquake (Franco, 2010; Franco, 2013; Goda, 2013; Goda, 2014; Pucciano et al. 2017; Franco et al.
127 2018) and tsunamis (Goda et al. 2018). Sect. 4 applies the framework presented to an application case study in Japan
128 where a regional (or national) entity may desire to adopt this type of risk transfer mechanism to help offset costs
129 associated with ash-fall generated by an eruption of Mt. Fuji. Conclusions and final remarks are collected in Sect. 5
130 where we elaborate on the potential application of this type of tool in a generalized, volcanic, global setting.

131

132

133 2 Construction of a volcano risk model

134 Japan is one of the most volcanically active countries in the world. There are 111 active volcanoes in Japan; on
135 average, a total of 15 volcanic events (including eruptions) occur every year, some of which seriously hinder human
136 life (JMA, 2019). Five Japanese cities, Tokyo, Osaka, Nagoya, Sapporo and Fukuoka, are ranked among the top-20
137 cities most at risk from volcanic eruptions according to the Lloyd’s City Risk Index (Lloyd’s, 2018).

138 The development of a volcanic risk model for Japanese volcanoes allows improving our ability to quantify said risk
139 as a preliminary step to transferring it to the capital markets. The model focuses on physical damage of buildings
140 arising from significant deposition of volcanic ash (tephra). The geographic scope is limited to the highly populated
141 and industrialized Prefectures of Tokyo and Kanagawa, potentially affected by the surrounding six major volcanoes:
142 Fuji, Hakone, Asama, Haruna, Kita-Yatsugatake and Kusatsu-Shirane (see Fig. 1). The model presented does not
143 consider damage to contents, business interruption, or costs associated with ash fall clean up. Neither does it
144 consider other volcanic hazards such as lava flows, pyroclastic density currents, debris flows or avalanches. The
145 model is structured into four modules: hazard, vulnerability, built environment (or exposure), and loss calculation,
146 which are described in more detail in the following subsections.



147 **Figure 1: The geographic domain of the volcano ash fall model presented in this paper includes Tokyo and Kanagawa**
148 **Prefectures in Japan, and the six major volcanoes that can affect them, Fuji, Hakone, Asama, Haruna, Kita-Yatsugatake,**
149 **and Kusatsu-Shirane.**

150

151 *2.1 The hazard module*

152 The hazard module consists of a collection of 26,807 volcanic ash fall footprints, each of them associated with one
153 of the six modelled volcanoes and with an annual probability of occurrence (see Table 1).

154

155 **Table 1: Number of volcanic ash fall events included in the model (i.e. those ash fall events that impact the model's**
156 **geographical domain of Tokyo and Kanagawa prefectures) and associated annual probabilities of occurrence by volcano.**
157 **Ash fall events originated by these volcanoes that do not impact the model domain have been excluded from the counts.**

158 This original set of footprints was produced by Risk Frontiers in 2017, and was provided specifically for the purpose
159 of building the volcano risk model that we present in this paper, on an exclusive basis. Modelling was performed
160 using *tephra2* numerical model, which simulates the dispersion of ash fall from a volcanic source using mass
161 conservation and advection-diffusion equations (Bonadonna et al., 2005; Connor and Connor, 2006). Tephra
162 accumulation is computed for specified locations surrounding a volcano in load units ($\text{Kg}\times\text{m}^2$). The model takes
163 into account appropriate vertical wind speed and direction profiles, which in this case were generated from
164 reanalysis wind data (NCEP-DOE Reanalysis2; NOAA).

165 The interaction of volcanic ash fall with rainfall may lead to an increase in the weight of the earlier due to absorption
166 of water, leading to increased loads and consequently to potentially more severe damages of affected structures. In
167 order to consider the possibility of ash fall – producing eruptions being concurrent to rainfall, “wet” versions of the
168 footprints were produced, respecting the rainfall patterns in the region of interest. The methodology used to create
169 “wet” footprints follows that described by Macedonio and Costa, 2012, and rainfall data were supplied by JBA Risk
170 Management. This was in the form of 10,000 years of simulated daily precipitation that incorporates tropical
171 cyclone and non-tropical cyclone precipitation; derived by JBA as part of their Global Flood Event Set.

172 *2.2 The vulnerability module*

173 As mentioned prior, the model considers damage to buildings only (residential, commercial or industrial), arising
174 from the vertical loads imposed by tephra on the structures. The level of damage to a specific building depends on
175 the total ash load and on the structural characteristics of the building. For each building type (i.e. a defined
176 combination of construction type, building rise and roof pitch) the model uses a specific vulnerability function that
177 computes the probability of experiencing a certain level of damage (expressed as a damage ratio of cost of repair
178 versus total cost of replacement) for a given physical load value upon that structure. The vulnerability functions
179 were developed on the basis of several studies on the subject (Spence et al., 2005; Maqsood et al., 2014; Jenkins et
180 al., 2014; Jenkins et al., 2015; Blong et al., 2017) for building typologies common in the area (see Table 2). Given
181 the lack of data on roof type for individual structures, the model assumes probabilities of different roof types within
182 the exposure set (low, medium or high pitch) depending on the building occupancy, construction typology and
183 building rise.

184

185



186 **Table 2: Building types common in the Tokyo and Kanagawa Prefectures of Japan, for which specific vulnerability**
187 **functions were developed in the volcano risk model. RC-SRC stands by “Reinforced Concrete – Steel Reinforced**
188 **Concrete”.**

189

190 Examples of damage functions used in the volcano risk model are provided in Fig. 2 for two contrasting building types (different
191 construction type, building rise and roof pitch).

192

193 **Figure 2: Damage functions for two different building types considered in the volcano risk model (“RC-SRC” stands for**
194 **Reinforced Concrete- Steel Reinforced Concrete; “Med.” stands for Medium); source of these damage functions is**
195 **Maqsood et al., 2014.**

196

197 *2.3 The exposure and the built environment (BE) modules*

198 These two closely-related modules jointly define the characteristics and monetary values of the group of buildings
199 (“portfolio”) for which the model will produce risk metrics.

- 200 1) The exposure module consists of a database structure that allows the user to characterise the portfolio of
201 interest and upload those details to the risk model in a structured manner, to subsequently run it. The main
202 database fields relate to number of buildings and associated values (i.e. building replacement values),
203 geographical location of the buildings (supported geocoding levels include geographical coordinates, 5 and
204 7 digit Postal Codes and Prefecture), occupancy, construction type and building rise.
- 205 2) The BE module is a database that completes the information provided by the user, wherever it is
206 incomplete or not accurate enough. This database represents the built environment across the model
207 geographical domain, specifically, the number, characteristics and spatial distribution of the different
208 building types as described in Table 2. The purpose of this module is two-fold. On one hand it allows
209 defining the likely location of buildings geo-located at resolutions coarser than geographical coordinate, in
210 order to better characterise their relationship with the spatial distribution of the hazard. The BE distributes
211 buildings into a finer spatial resolution on a probabilistic basis, using weights that are specific to each
212 building type. Weights were computed on the basis of information such as land use and land cover type and
213 census data. In the case of our model, data sources included the 2013 Housing and Land Survey (Statistics
214 Bureau, Government of Japan), the 2014 Tokyo Statistical Yearbook (Tokyo Metropolitan Government),
215 Japan E-Stat (Ministry of Land, Infrastructure, Transport and Tourism), etc. The second purpose of the BE
216 is to infer damage-relevant characteristics of buildings (e.g. building rise, construction type, etc.) if this
217 information is not captured in the description of the buildings we want to model. This is again done on a
218 probabilistic basis, depending on the location of the building and any known characteristics (e.g. building
219 occupancy).

220

221 *2.4 The loss calculation module*

222 The loss calculation module or engine estimates the monetary loss associated to each building for the different
223 events that can potentially affect it. This is attained (for each event-building “interaction”) by multiplying the
224 damage ratio prescribed by the corresponding vulnerability function and the replacement value of the building,
225 which needs to be provided by the modeller. The loss calculation module allows reporting losses by building and by
226 event; as well as by event (aggregate event loss).



227 Volcanic loss data are very scarce due to the low frequencies of damaging eruptions. We used a few independent
228 sources to validate modelled losses. These included two studies on damage estimations of a repeat of the 1707 Fuji
229 eruption (Kuge et al., 2016; Cabinet Office of Japan, 2002) that were used to validate modelled losses from severe
230 eruptions. To validate modelled losses from less severe eruptions, we used as a proxy data on insured building losses
231 caused by loading of snow in Toyo and nearby Prefectures in February 2014 (General Insurance Association of
232 Japan, 2015). Kuge et al. (2016) modelled losses for industrial buildings (with an assumed value of 1 Billion JPY
233 per building) if there was a repeat of the Fuji 1707 eruption. Estimated individual building losses ranged between 35
234 and 180 Million JPY (K. Kuge, personal communication, 2017). This compares well with our modelled losses
235 between 28.6 and 138.4 Million JPY for industrial buildings, under a reconstruction of the Fuji 1707 eruption.
236 Regarding Residential buildings, the reported average building loss value for the February 2014 snowfall event in
237 Japan was 1.2 Million JPY (General Insurance Association of Japan, 2015). Assuming a snow density value of 200
238 kg/m³, we identified ash fall events in the volcano model producing equivalent loads, and calculated an average
239 Residential building loss of 1.7 Million JPY.

240

241 3 Design of a parametric trigger for volcano risk transfer

242 A parametric trigger refers to a specific value or threshold of a physical, measurable characteristic associated to the
243 natural phenomenon in question (e.g. to ash fall-producing volcanic eruptions in this case, or earthquakes,
244 hurricanes, etc.), above which a significant level of damage of exposed assets (e.g. damage to buildings) is likely to
245 occur. When the physical parameter exceeds that threshold for a particular event, it is considered that a risk cedant
246 should receive a payment commensurate to the loss that their portfolio will likely incur as a result of being exposed
247 to the event.

248 Therefore, when designing a parametric risk transfer mechanism, it is crucial to select a physical parameter that
249 correlates well with potential losses. In the case of parametric earthquake risk transfer, for instance, it is common to
250 select the magnitude of the earthquake as the main parameter, and subsequently define threshold value/s for the
251 magnitude scale, above which significant damages are likely to occur (Franco, 2010; Franco, 2013). Other
252 alternatives used in practice consider shaking measurements such as peak ground accelerations or spectral
253 accelerations at a set of locations (Goda, 2013; Goda, 2014; Pucciano et al. 2017).

254 There are three important requirements for the selection of a physical characteristic of a natural phenomenon to be
255 used as a parametric trigger in the design of a risk transfer mechanism:

- 256 1) The parameter must exhibit strong correlation to losses incurred as a consequence of the physical phenomenon.
- 257 2) The parameter needs to be measured and reported by a reliable and impartial organisation on a near-real time
258 basis. In the case of earthquakes, for instance, earthquake information is often obtained from reliable
259 international bodies such as the U.S. Geological Survey (Wald & Franco, 2017).
- 260 3) Finally, each of the stochastic events in the catastrophe risk model used as a basis to design the risk transfer
261 solution must explicitly include the corresponding value for the selected physical parameter. In the case of
262 earthquake risk transfer, for instance, each of the earthquake events in the catastrophe risk model needs to be
263 described by its magnitude (if this is the metric of choice for the trigger conditions).

264 3.1 Choosing the trigger parameters for volcanic eruptions

265 In our case study, we have researched several physical parameters associated to the phenomenon of volcanic ash
266 falls, as well as Japanese organizations reporting this type of information on a real-time basis while a volcanic
267 eruption unfolds. In Japan, the Japanese Meteorological Agency (JMA) operationally monitors volcanic activity
268 throughout the country and issues relevant warnings and information to mitigate related damages. To continuously
269 monitor volcanic activity, JMA deploys seismographs and related observation instruments in the vicinity of 50



270 volcanoes that are remarkably active in Japan. When volcanic anomalies are detected, the Agency steps up its
271 monitoring/observation activities and publishes volcanic information and regular bulletins; mainly “Observation
272 Reports on Eruption” and “Volcanic Ash Fall Forecasts” (VAFFs). The Observation Reports and VAFFs are
273 published on a real-time basis for all active volcanoes in Japan; however they contain different types of information.
274 Observation Reports provide information on the ongoing eruption, such as eruption time, eruptive column height (in
275 meters above the crater), the main direction of movement of the eruptive plume at the moment of the report (as per
276 eight cardinal directions: N, E, SE, etc....), and the maximum plume height recorded from the onset of the eruption
277 (Hasegawa et al., 2015). On the other hand, the VAFFs consist of modelled (not observed) ash fall areas and
278 amounts, and are produced when heavy (> 1 mm) or moderate (0.1-1 mm) ash quantities are forecasted in principle.
279 These maps correspond to the moment when the VAFF is issued, and cumulative ash fall map products (i.e. the total
280 accumulated ash fall on the ground throughout the eruption) are not released by JMA.

281 Eruptive column height values are available for each eruptive event present in the volcano risk model. In addition,
282 we estimate the predominant direction of movement of the eruptive plume for each event by assuming it coincides
283 with the main axis of ash fall deposition on the ground. Therefore, we calculate the main direction of deposition of
284 ash fall for each of the event footprints in the model by performing spatial analyses. Resulting azimuths were
285 classified into eight directional sectors (N, NE, E, SE, S, SW, W, and NW) and used as a proxy for the main
286 direction of movement of the generating eruptive ash plume.

287 Based on the above, we selected a combination of two eruption-related parameters (reported eruptive column height
288 and direction of movement of the eruptive plume) for the design of our parametric trigger, since:

- 289 1) These two parameters are reported by JMA on a near-real time basis when an eruption occurs.
- 290 2) The height of the eruptive column and preferential direction of movement of eruptive plume for each of the
291 stochastic events in the model can be assigned based on existing datasets.
- 292 3) We found a significant relationship between eruptive column height and losses as modelled by the volcano
293 risk model (Fig. 3). Pearson correlation tests were performed between eruptive column height and losses,
294 for eight subsets of eruptive events with defined eruptive plume directions (i.e. E, N, NE, NW, S, SE, SW,
295 W). Resulting p-values were all smaller than $\alpha = 0.05$, indicating a significant correlation between
296 eruptive column height and losses for all directional sectors.

297 We do not consider modelled ash fall areas for the parametric design, given that cumulative maps are not made
298 typically available and it is thus not straightforward to establish a relationship with losses.

299

300 **Figure 3: Relationship between height of eruptive column (in Km, from crater rim) and modelled losses for all eruptive**
301 **events in the volcano risk model. Each panel displays a subset of eruptions featuring a specific predominant direction of**
302 **their eruptive plume (East, North, North-East, North-West, South, South-East, South-West and West).**

303

304 3.2 Choosing the trigger type

305 The next step consists of designing the parametric trigger on the basis of the two physical eruptive parameters
306 selected. We have however, several choices in the formulation of such a trigger (Wald & Franco, 2016; Pucciano et
307 al., 2017). In this paper, we focus on two simple variants:

- 308 1) *Binary triggers*, for which each event of the stochastic catalogue can either pay or not pay a fixed monetary
309 amount, P , depending on whether it exceeds the parameter threshold defined by the specific design.



310 2) *Multilayer triggers*, for which each event can pay one of N predefined payment levels, associated to a series
311 of defined parameter thresholds.

312 The binary trigger can be seen as a particular case of a multilayer trigger with $N = 1$. As treatment of this case is
313 easier, we start with the design of a binary parametric trigger and we later generalize it to N payment levels.

314 Since we are building a trigger using plume height and ash plume direction expressed as per eight wind sectors (N,
315 NE, E, SE, S, SW, W, NW), it is natural to represent the trigger simply as a set of threshold plume height values for
316 each wind sector, $\{H_s\}_{s \in W}$, where W is the set of the possible wind sectors.

317 This means that if an event i has plume height h_i and wind sector s_i , it triggers a payment if and only if $h_i \geq H_{s=s_i}$,
318 which is the *trigger condition*.

319 We can model the behaviour of the trigger using the stochastic events in the volcano risk model. Let's call T the set
320 of the stochastic events fulfilling the trigger conditions. Since they are the only events releasing a payment, their
321 exceedance rate, collectively, defines the payment occurrence rate.

$$R = \sum_{i \in T} r_i$$

322 where r_i stands for the event occurrence rate. From the trigger rate we obtain the yearly triggering probability as
323 $p = 1 - e^{-R}$ as usual for a Poisson process. The expected payment in a year can be expressed either as $EP = p \cdot P$
324 or $EP = R \cdot P$ but since we generally have $p \sim R$ the impact of the difference is minimal.

325 If we interpret the trigger as insurance, the EP would correspond to the *pure premium* of the policy, which is a
326 quantity somewhat proportional to its price. Thus, the more often the trigger is activated the more expensive it is.
327 Given a certain trigger payment and a certain yearly budget, we can thus derive a target triggering rate R^* .

328 Since the trigger pays a fixed amount, it will always provide either too much money or too little, if compared to the
329 actual event loss. This difference is expressed via the following quantity, called **basis risk**, which we define based
330 on Franco (2010) as:

$$BR = BR_+ - BR_- = \sum_{i: l_i < P} (P_i - l'_i) r_i - \sum_{i: l_i > P_i} (l'_i - P_i) r_i$$

331 Where $P_i = P$ if $i \in T$ and 0 otherwise and l'_i represent the loss component in the loss layer of interest. The first
332 (second) term is called positive (negative) basis risk.

333 3.3 Optimization of the trigger

334 The standard approach to trigger design consists of choosing the trigger thresholds such that basis risk is minimized
335 (Franco, 2010; Goda, 2013; Goda, 2014; Pucciano et al., 2017). Since the budget and the trigger recovery do tend to
336 change during the design process, recent approaches have considered the alternative objective that the trigger simply
337 maximizes the amount of **risk transfer** (Franco et al., 2018; Franco et al., 2019), i.e. find T that maximizes the
338 quantity defined as:

$$K = \sum_{i \in T} r_i l_i$$



339 Where l_i is the loss for event i , that is, we want a trigger which is activated by those events in the catalogue that
 340 collectively have the greater expected annual loss. Maximizing the risk transfer is quite apt, since it states clearly
 341 that the trigger is designed to be activated on the set of events that affect the policy holder the most.

342 Using the trigger condition we can rewrite the risk transfer equation in function of the trigger parameters as

$$K(\{H_s\}_{s \in W}) = \sum_{s \in W} \rho_s(H_s) = \sum_{s \in W} \sum_{i: h_i \geq H_s = s_i} r_i l_i \quad (1)$$

343 Where $\rho_s(H_s)$ is the risk transferred by all the events in sector s , which is a function of the threshold value for that
 344 sector, H_s .

345 If we discretize the possible values of H_s in a vector, H_s^k , and we compute all the possible values of $r t_s$ for this
 346 vector, $\rho_s^k = \rho_s(H_s^k)$, we can rewrite the risk transferred per sector as

$$\rho_s(H_s) = \sum_k x_s^k \rho_s^k \quad (2)$$

347 Where x_s^k is a vector of 0 and one single 1 placed at the index k' such that $H_s^{k'} = H_s$. This means that we can write
 348 H_s as

$$H_s = \sum_k x_s^k H_s^k$$

349 When plugging Eq. (2) in Eq. (1), the risk transfer equation becomes

$$K = \sum_{s \in W} \sum_k x_s^k \rho_s^k$$

350 It seems an over complication of a previously simple equation, but actually we eliminated the sum over $i \in T$. Now
 351 the unknown is moved from the set T to the vectors x_s which resembles a problem of linear algebra (it's not, given
 352 the particular form of the vectors, but it's still easier to approach than before). We can now apply similar
 353 considerations to the rate equation obtaining an expression for the payment occurrence rate

$$R = \sum_{s \in W} \sum_k x_s^k \lambda_s^k$$

354 where $\lambda_s^k = \sum_{i: h_i \geq H_s^k} r_i$. At this point we can re-write the trigger design as the following optimization problem:

find the x_s^k

which maximize $\sum_{s \in W} \sum_k x_s^k \rho_s^k$

subject to the following constraints:

$$\sum_{s \in W} \sum_k x_s^k \lambda_s^k \leq R^*$$

$$\sum_k x_s^k H_s^k - \sum_k x_{s'}^k H_{s'}^k \leq \Delta H \quad \forall \text{ adjacent } s, s'$$



$$\sum_k x_s^k = 1 \quad \forall s$$

$$x_s^k \in \{0, 1\}$$

355 Where R^* is the target trigger rate and ΔH is a maximum threshold difference between two adjacent wind sectors.
 356 Limiting this difference is a way to take into account epistemic risk, that is, risk induced by using a particular model.
 357 It is also a way to decrease trigger sensitivity to the wind sector parameter.

358 The last two constrains, instead, are just a way to express the peculiar form of the x_s vectors.

359 The problem, thus stated, can be solved with linear programming techniques (Franco et al., 2019) or with other
 360 alternative methods (De Armas et al., 2016). The problem is solved in this paper using standard Python libraries for
 361 mixed integer linear programming.

362 As can be seen from the equations for K and R , these two quantities are non-decreasing when the number of trigger
 363 events increases. Thus, maximizing K involves increasing the number of events captured by the trigger (by
 364 decreasing the threshold values) up to a certain point where the critical value R^* is reached. This constraint, as all
 365 the other constraints of the optimization, imposes a trade-off to the $\max(K)$. The curve described by $\max(K)$ in
 366 function of R^* is a Pareto front, an example of which is depicted in Fig. 4.

367

368 **Figure 4: Pareto front for a binary trigger designed modelling stochastic losses for Mt. Fuji. The transferred risk is**
 369 **displayed as percentage of the total risk.**

370

371 In a multi-layer payment trigger, instead of having one single threshold height value we have a series of threshold
 372 values for each wind sector. Each threshold value pays a certain fraction of the maximum payment. Let's suppose
 373 we can generate a two-layer trigger. We decide in advance that the occurrence rate of the first and second payment
 374 will be R_1^* and R_2^* respectively, with $R_1^* > R_2^*$.

375 To build the trigger we follow these steps.

- 376 1) We build a binary trigger, $\{H_s^{(1)}\}_{s \in W^*}$, with occurrence rate R_1^*
 377 2) We build a second trigger with occurrence rate R_2^* . The problem is identical to the binary one, but with an
 378 additional constraint:

$$\sum_k x_s^k H_s^k > H_s^{(1)} \quad \forall s$$

379 Which means that each threshold must be greater or equal to the threshold for that sector in the lower layer. It is easy
 380 to generalise to N layers imposing at each layer n the constraint $H_s^{(n)} > H_s^{(n-1)} \quad \forall s$.

381

382 4 Application and Results

383 For this application, we consider a case where a cedant such as a regional Government may want to consider
 384 financing the risk of economic losses arising from damage to citizens' residential properties in the Prefectures of
 385 Tokyo and Kanagawa, caused by the potential occurrence of damaging eruptive ash fall events. We assume that the



386 Government has an implicit need to help reconstruct citizens' dwellings after a catastrophic volcanic event, and may
387 therefore want to consider adopting a parametric risk transfer solution appropriately designed for these cases.

388 The first step consisted of putting together a comprehensive "portfolio" of residential properties for the modelled
389 geographical area (Tokyo and Kanagawa Prefectures). This portfolio is the input that needs to be provided to the
390 volcano risk model, for it to calculate potential losses on a probabilistic basis. To do so, we used the census data
391 incorporated in the model database, which consists of the number of dwellings by administrative unit (Shiku) and by
392 type of residential occupancy (single family or condominium). The cost of rebuilding each of the properties also
393 needs to be provided to the model, and we used different information sources to estimate representative rebuilding
394 costs for single family dwellings and condominiums in the prefectures of Tokyo and Kanagawa (Table 3).

395

396 **Table 3: Representative reconstruction values have been estimated on the basis of several sources of information,**
397 **including data on building construction values from Japanese Government Statistics (<https://www.e-stat.go.jp>) and**
398 **insured building values from the General Insurance Rating Organization of Japan (<https://www.giroj.or.jp>).**

399

400 Table 4 provides a summary of the total number of dwellings and corresponding total reconstruction values for the
401 modelled portfolio.

402

403 **Table 4: Total number of dwellings and total reconstruction values modelled in the volcano risk model for six Japanese**
404 **volcanoes (by prefecture, and totals). Number of dwellings from Japanese Government Statistics ([https://www.e-](https://www.e-stat.go.jp)**
405 **stat.go.jp); Total Values have been calculated on the basis of representative reconstruction values in Table 3.**

406

407 The volcano risk model was run and results were extracted as an "Event Loss Table" or "ELT" (i.e. losses produced
408 by each of the volcanic ash fall events included the model, on the residential portfolio considered). Table 5 provides
409 an example of results for a few ash fall events from Mt. Fuji. Losses can be equal to zero for events either impacting
410 areas outside the model's geographical domain (i.e. Tokyo and Kanagawa prefectures), or impacting geographical
411 areas within the model domain that have no (modelled) buildings located in them.

412

413 **Table 5: Subset of ELT outputs from the volcano risk model, run of the residential portfolio described. The table shows**
414 **losses on the portfolio caused by four of the model's ash fall events from Mt. Fuji. The mean loss and the standard**
415 **deviation of the loss distribution associated to each event (in JPY) are reported in the ELT.**

416

417 The ELT results were used to analyse the correlation between height of eruptive column and modelled event losses
418 (Fig. 3), which is a pre-requisite for the selection of this metric for the design of the parametric trigger. Figure 3
419 plots, for each modelled ash fall event, the height of the eruptive plume (x axis) versus the logarithm of the modelled
420 loss (y axis), showing a strong correlation between the two. Each panel in Fig. 3 depicts eruptive events featuring a
421 specific predominant dispersal direction of their eruptive plume (East, North, North-East, North-West, South, South-
422 East, South-West and West). The correlation between plume height and loss holds for all direction sectors.
423 Dispersion in the plot is due to the fact that the severity of loss, despite being strongly correlated with plume height
424 and plume direction, also depends on other factors, such as duration of the eruption, size distribution of eruptive
425 particles, etc.



426 Calculation of Annual Average Losses (AAL) for the modelled portfolio on a per-volcano basis (Fig. 5, left) shows
427 that Mt Fuji is the main risk source, its average AAL amounting to more than 1 billion JPY per year. Therefore,
428 we chose Mt. Fuji for the calculation of the parametric risk transfer structure. Being located westward of the
429 exposure domain, risk associated to Mt. Fuji is mainly concentrated in the eastern wind sector. In particular, the only
430 sectors containing risk are NE, E, SE, S and SW, even if the last three only in minimal part (Fig. 5, right).

431

432 **Figure 5: (Left) Modelled AAL for the six volcanoes included in the volcano risk model. (Right) Breakdown of Mt Fuji**
433 **risk by wind sector.**

434

435 The occurrence exceeding probability curve (OEP) derived from the modelled losses for Mt. Fuji is depicted in Fig.
436 6. As an example, we imagine that the policy holder might be interested in covering all losses exceeding 30 Billion
437 JPY with a parametric coverage releasing two possible payment levels of 100 and 300 Billion JPY. This means

$$l'_i = \min(\max(l_i - 30B, 0), 300B)$$

438 We choose the target exceedance rates for these layers to match the corresponding return period on the OEP curve,
439 3862 and 4944 years. In this way we end up with the trigger OEP curve depicted in Fig. 6.

440 We also imposed a plume height discretization of 1Km, i.e. $H_s^k = (1\text{Km}, 2\text{Km}, \dots, 50\text{km})$ and a maximum threshold
441 difference between adjacent sectors $\Delta H = 4\text{Km}$.

442

443 **Figure 6: OEP curve for Mt Fuji losses (blue) and trigger payments (orange)**

444

445 The result of the optimization algorithm is depicted in Fig. 7. The (wind sector, plume height) plane is divided into
446 three payment regions, separated by the two trigger layers. As expected, the plume height thresholds are smaller for
447 regions of high risk. The smoothing condition ensures that there is coverage also in the sectors that are adjacent to
448 the sectors at risk, in case that an event has ash fall direction close to the border between two sectors and it is
449 categorized wrongly.

450

451 **Figure 7: Parametric Trigger for Mt. Fuji Each dashed line correspond to a unit of 10Km**

452

453 Table 6 summarizes the results of the parametric trigger design for the considered cover, including the plume height
454 thresholds by wind sector for the two Layers defined, and the corresponding proportion of risk transferred and layer
455 payments.

456

457 **Table 6: Parametric trigger for Mt Fuji. The risk transferred by each layer is expressed as percentage over the total risk**
458 **of Mt Fuji. The layer payment is expressed as fraction of the maximum payment (300 Billion JPY).**

459



460 The net basis risk of the trigger is 7 Million JPY / year, sum of 32 Million JPY / year of positive and 25 Million JPY
461 / year of negative basis risk, while the expected recovery is of 87 Million JPY / year. The prevalence of basis risk is
462 expected, since the OEP curve of the bond sits on top of the losses OEP in the layer of interest (30 Billion – 330
463 Billion JPY). This amount can be fine-tuned increasing the return periods of the layers until comfortable levels of
464 basis risk are reached.

465 5 Conclusions

466 We present a novel methodology to parameterize financial risk transfer instruments for explosive, tephra fall-
467 producing volcanic eruptions. The design of the parametric product relies on easily obtainable, observable physical
468 parameters relating to explosive volcanic eruptions; namely maximum observed height of the eruptive column and
469 the prevalent direction of dispersal of the associated ash plume.

470 We take as a case study Mount Fuji in Japan, the largest and closest active volcano to the populous Tokyo
471 metropolitan area and the heavily industrialized Kanagawa prefecture (Yamamoto & Nakada, 2015). In Japan, the
472 JMA reports height of the eruptive column and the predominant direction of ash dispersal as part of the
473 “Observation Reports on Eruption” that are released for any erupting volcano on a near-real time basis. The design
474 of the parametric risk transfer for our case study relies on Guy Carpenter’s fully probabilistic model for volcanic
475 eruptions potentially affecting Tokyo and Kanagawa prefectures, which includes 10,000 simulated volcanic ash fall
476 events arising from explosive eruptions of different sizes at Mount Fuji. Therefore, the second pre-requisite for the
477 successful design of an equivalent parametric product elsewhere is the existence of a fully probabilistic eruptive loss
478 model encompassing the range of all possible eruptive events of interest, and incorporating information relating to
479 plume height and predominant direction of ash fall dispersal for each event.

480 For the parametric design, we focused on explosive eruptions producing significant tephra loads capable of
481 generating property damages (these are the type of eruptive events considered by the volcano risk model). The
482 resulting parametric product could be of interest to a number of organizations, including regional and national
483 Governments, but also to economic sectors such as insurers of commercial and industrial properties in these
484 Prefectures (insurance cover for volcanic eruptions is included as part of the standard earthquake policies in Japan).
485 In our case study, we took as an example a “portfolio” of residential properties representing the existing residential
486 building stock in the Tokyo and Kanagawa prefectures. These could be severely affected by a significant eruption
487 from Mount Fuji- the last Fuji eruption in year 1707 is a good example - thus potentially generating a financial
488 burden for the regional and/or or national Governments.

489 We designed a multi-layer trigger assuming that a policy holder might be interested in covering all losses exceeding
490 30 Billion JPY, with a coverage releasing two possible payment levels of 100 and 300 Billion JPY provided the
491 appropriate trigger conditions of eruptive column height and predominant plume direction are met (Table 6). This
492 product would provide a policy holder such as a regional Government a quick way to access cash to help repair
493 damages incurred by dwellings as a consequence of a major volcanic eruption.

494 Further work on the design of volcano-related parametric risk transfer products may relate to different aspects. On
495 one hand, and also considering ash fall-producing volcanic eruptions, the design may be extended to consider other
496 types of damages such as those to crops and livestock, costs arising from ash fall clean up and disposal in urban
497 areas and roads, Business Interruption costs arising from air traffic disruption, airport closures and disruption of
498 critical infrastructures including transportation networks, electricity, water supplies and telecommunications, etc.
499 (Wilson et al., 2012). For any of these types of losses, specific ash fall vulnerability functions must be incorporated
500 in the fully probabilistic volcano model considered. The parametric design presented in this paper could be adapted
501 to coverage of these types of losses, provided a strong correlation was also found between eruptive column height
502 and main direction of ash dispersal and modelled losses.



503 On the other hand, despite ash fall is the volcanic peril with the largest potential of causing wide spread losses (since
504 it is by far the most widely distributed eruptive product), there are other volcanic perils that have a large destructive
505 potential, albeit with a more constrained spatial reach. These include lava flows, pyroclastic density currents, lahars,
506 volcano flank collapses and ballistic blocks. Design of parametric transfer products for these volcano hazards would
507 entail a rather different approach; concerning both the modelling of losses (starting with the incorporation of these
508 specific hazard events to the fully probabilistic volcano model), to the selection and monitoring of hazard-related
509 trigger parameters.

510 There are several features of the design presented that make it potentially applicable to other volcanic settings where
511 explosive volcanism is typical. In particular, the choice of eruption-related parameters (height of eruptive column
512 and preferential direction of dispersal of ash fall) means that no special monitoring equipment is needed for
513 recordings. On the other hand, it is important that an official, reputable national or regional agency reports such
514 observations in a reliable and timely manner. Implementation should be straight forward in countries with
515 established volcano observatories. In others, it could be interesting to explore global monitoring solutions like
516 satellite-based remote sensing to report both column height and preferential direction of ash fall dispersal on a near
517 real time basis. Such arrangement would provide for a centralised, consistent and independent monitoring solution
518 applicable to explosive eruptions world-wide.

519 The other important requisite that needs to be in place is a suitable volcano risk model that produces stochastic loss
520 outputs associated to ash fall-producing eruptions. In an insurance context, availability of such models is still rare.
521 Nonetheless, increased collaboration between academic experts and the insurance industry brings all the necessary
522 elements together for the creation of such models, as it has been in the case presented in this paper. Whereas
523 building of volcano loss models requires from a non-negligible investment of time and resources, the availability of
524 open-source hazard simulation models such as tephra2 and of global open databases (e.g. wind data, eruptive data,
525 etc.) means that the ingredients needed for development are pretty much available on a world-wide basis. Scaling up
526 such approach in order to model a significantly larger number of volcanoes than presented in this paper is currently
527 being looked into, with promising preliminary results. Increased interest in parametric risk transfer products from
528 the insurance industry and capital markets is helping build momentum for the development of risk models of “non-
529 traditional” perils such as volcanic eruptions, and the design of associated risk transfer mechanisms.

530

531

532

533

534

535

536

537

538

539

540



541 **References**

- 542 Artemis (online blog on catastrophe bonds, insurance-linked securities and alternative reinsurance capital). Sompo
543 Japan to launch parametric volcanic risk insurance [Available [http://www.artemis.bm/news/sompo-japan-to-launch-](http://www.artemis.bm/news/sompo-japan-to-launch-parametric-volcanic-risk-insurance/)
544 [parametric-volcanic-risk-insurance/](http://www.artemis.bm/news/sompo-japan-to-launch-parametric-volcanic-risk-insurance/)], 2016.
- 545 Blong, R.J., Grasso, P., Jenkins, S.F., Magill, C.R., Wilson, T.M., McMullan, K. and Kandlbauer, J.: Estimating
546 building vulnerability to volcanic ash fall for insurance and other purposes. *Journal of Applied Volcanology*, 6:2, 1-
547 13, doi: 10.1186/s13617-017-0054-9, 2017.
- 548 Bonadonna, C., Costa, A., Folch, A., and Koyaguchi, T.: Tephra dispersal and sedimentation. In: Sigurdsson H,
549 Houghton B, McNutt S, Rymer H, Stix J (eds) *Encyclopedia of volcanoes*, 2nd edn. Elsevier, 587–597, doi:
550 10.1016/B978-0-12-385938-9.00033-X, 2015b.
- 551
552 Cabinet Office of Japan: Damage estimation of a historic eruption of Mt. Fuji. Cabinet Office of Japan, 124p. (in
553 Japanese), <http://www.bousai.go.jp/kazan/fujisan-kyougikai/report/pdf/houkokusyo7.pdf>, 2002.
- 554
555 Connor, L.J., Connor, C.B.: Inversion is the key to dispersion: understanding eruption dynamics by inverting tephra
556 fallout. In: Mader, H.M., Coles, S.G., Connor, C.B., Connor, L.J. (eds) *Statistics in volcanology*. IAVCEI
557 Publications, Geological Society of London, 231–242, doi: 10.1144/IAVCEI001.18, 2006.
- 558
559 Cummins, J.D.: CAT Bonds and Other Risk-Linked Securities: State of the Market and Recent Developments. *Risk*
560 *Management and Insurance Review*, 11, 23-47, doi: 10.1111/j.1540-6296.2008.00127.x, 2008.
- 561 de Armas J., Calvet L., Franco G., Lopeman M., Juan A.A.: Minimizing Trigger Error in Parametric Earthquake
562 Catastrophe Bonds via Statistical Approaches, in León, R., Muñoz-Torres, M., Moneva, J. (eds) *Modeling and*
563 *Simulation in Engineering, Economics and Management*. Lecture Notes in Business Information Processing,
564 Springer, Cham, 254, 167-175, doi: 10.1007/978-3-319-40506-3_17, 2016.
- 565 Franco, G.: Minimization of Trigger Error in Cat-in-a-Box Parametric Earthquake Catastrophe Bonds with an
566 Application to Costa Rica. *Earthquake Spectra*, 26 (4), 983-998, doi: 10.1193/1.3479932, 2010.
- 567 Franco, G.: Construction of customized payment tables for cat-in-a-box earthquake triggers as a basis risk reduction
568 device, in *Proceedings, 11th International Conference on Structural Safety & Reliability*, Taylor & Francis Group,
569 New York, doi: 10.1201/b16387-793, 2013.
- 570
571 Franco, G.: Earthquake mitigation strategies through insurance, in *Encyclopedia of Earthquake Engineering*,
572 Springer Berlin Heidelberg, 1–18, doi: 10.1007/978-3-642-36197-5_401-1, 2014.
- 573
574 Franco, G., Guidotti, R., Bayliss, C., Estrada, A., Juan, A. A., Pomonis, A.: Earthquake Financial Protection for
575 Greece: A Parametric Insurance Cover Prototype, in *Proceedings, 2nd International Conference on Natural Hazards*
576 *& Infrastructure*, Chania, Greece, 2019.
- 577
578 Franco, G., Tirabassi, G., Lopeman, M., Wald, D.J., and Siembieda, W.J.: Increasing earthquake insurance coverage
579 in California via parametric hedges. In *Eleventh US National Conference on Earthquake Engineering*, 2018.
- 580
581 General Insurance Association of Japan, Claims associated to weather events.
582 <http://www.sonpo.or.jp/news/statistics/disaster/weather/index.html#2016>, 2015.
- 583 GVP (Global Volcanic Program), Smithsonian Institution. <https://volcano.si.edu/volcano.cfm?vn=264040>, last
584 access: 12 March 2019.



- 585 Goda, K.: Basis risk for earthquake catastrophe bond trigger using scenario-based versus station intensity-based
586 approaches: A case study for southwestern British Columbia, *Earthquake Spectra*, 29, 757-775, doi:
587 10.1193/1.4000164, 2013.
588
- 589 Goda, K.: Seismic risk management of insurance portfolio using catastrophe bonds, *Computer-Aided Civil and*
590 *Infrastructure Engineering*, 30, 570–582, doi: 10.1193/1.4000164, 2014.
591
- 592 Government of Japan: Mt. Fuji volcanic disaster prevention measures, [Available at
593 <http://www.bousai.go.jp/kazan/fujisan-kyougikai/report/pdf/houkokusyo7.pdf>], 2004.
- 594 Hasegawa, Y., Sugai, A., Hayashi, Y., Hayashi, Y., Saito, S. and Shimbori, T.: Improvements of volcanic ash fall
595 forecasts issued by the Japan Meteorological Agency. *Journal of Applied Volcanology*, 4 (2), 1-12, doi:
596 10.1186/s13617-014-0018-2, 2015.
- 597 Jenkins, S., Spence, R., Fonseca, J., Solidum, R., and Wilson, T.: Volcanic risk assessment: Quantifying physical
598 vulnerability in the built environment. *Journal of Volcanology and Geothermal Research*, 276, 105-120, doi:
599 10.1016/j.jvolgeores.2014.03.002, 2014.
- 600 Jenkins, S., Wilson, T.M., Magill, C.R., Miller, V., Stewart, C., Marzocchi, W. and Boulton, M.: Volcanic ash fall
601 hazard and risk: Technical Background Paper for the UNISDR 2015 Global Assessment Report on Disaster Risk
602 Reduction. *Global Volcano Model and IAVCEI*. [Available at www.preventionweb.net/english/hyogo/gar/], 2015.
- 603 JMA (Japanese Meteorological Agency): Monitoring of Volcanic Activity.
604 <https://www.jma.go.jp/jma/en/Activities/earthquake.html>, last access: 12 March 2019.
- 605 Kuge, K., Kawabe, K. and Horie, K.: Proposal for Risk Assessment Method of Volcanic Eruption Damage
606 Estimation of Industrial Facilities against 1707 Hoei Volcano Level (Part 2), *Summaries of Technical Papers of*
607 *Annual Meeting, Architectural Institute of Japan, Structure I*, 08, 69-70, 2016.
- 608 Lloyd's and Cambridge Centre for Risk Studies. *Lloyd's City Risk Index 2018*. [Available
609 at lloyds.com/cityriskindex/], 2018.
- 610 Macedonio, G. and Costa, A.: Brief Communication "Rain effect on the load of tephra deposits", *Nat. Hazards Earth*
611 *Syst. Sci.*, 12, 1229-1233, doi: 10.5194/nhess-12-1229-2012, 2012.
- 612 Maqsood, T., Wehner, M., Ryu, H., Edwards, M., Dale, K. and Miller, V.: GAR15 Regional Vulnerability
613 Functions: Reporting on the UNISDR/GA SE Asian Regional Workshop on Structural Vulnerability Models for the
614 GAR Global Risk Assessment, 11–14 November, 2013, *Geoscience Australia, Canberra, Australia*, doi:
615 10.11636/Record.2014.038, 2014.
- 616 Newhall, C. and Self, S.: The Volcanic Explosivity Index (VEI): An Estimate of Explosive Magnitude for Historical
617 Volcanism. *Journal of Geophysical Research*, 87, 1231-1238, doi: 10.1029/JC087iC02p01231, 1982.
- 618 NOAA/OAR/ESRL PSD: NCEP-DOE Reanalysis 2 data. [Available at <https://www.esrl.noaa.gov/psd/>]
- 619 Oppenheimer, C.: Climatic, environmental and human consequences of the largest known historic eruption:
620 Tambora volcano (Indonesia) 1815. *Progress in Physical Geography: Earth and Environment*. 27 (2), doi:
621 10.1191/0309133303pp379ra, 230-259, 2003.
- 622 Oxford Economics: The economic impacts of air travel restrictions due to volcanic ash. *Oxford Economics, Oxford*.
623 [Available at <https://www.oxfordeconomics.com/my-oxford/projects/129051>], 2010.
624



- 625 Pucciano, P, Franco, G, Bazzurro, P.: Loss Predictive Power of Strong Motion Networks for Usage in Parametric
626 Risk Transfer: Istanbul as a Case Study. *Earthquake Spectra*, 33-4, 1513-1531, doi: 10.1193/021517EQS032M,
627 2017.
628
- 629 Self, S., Rampino, M.R., Newton, M.S. and Wolff, J.A.: Volcanological study of the great Tambora eruption of
630 1815. *Geology*, 12 (11), 659–663. doi: [10.1130/0091-7613\(1984\)12<659:VSOTGT>2.0.CO;2](https://doi.org/10.1130/0091-7613(1984)12<659:VSOTGT>2.0.CO;2), 1984.
631
- 632 Spence, R.J.S., Kelman, I., Calogero, E., Toyos, G., Baxter, P.J., Komorowski, J.C.: Modelling expected physical
633 impacts and human casualties from explosive volcanic eruptions. *Natural Hazards and Earth System Sciences*, 5 (6),
634 1003-1015, doi: 10.5194/nhess-5-1003-2005, 2005.
635
- 636 Stothers, R.B.: The great Tambora eruption in 1815 and its aftermath. *Science*, 224, 1191-1198, doi:
637 10.1126/science.224.4654.1191, 1984.
638
- 639 Swiss Re: The Fundamentals of Insurance-Linked Securities [Available at [https://www.swissre.com/Library/ils-the-](https://www.swissre.com/Library/ils-the-fundamentals-of-insurance-linked-securities.html)
640 [fundamentals-of-insurance-linked-securities.html](https://www.swissre.com/Library/ils-the-fundamentals-of-insurance-linked-securities.html)], 2011.
641
- 642 Wald, D.J., and Franco, G.: Money Matters: Rapid post-earthquake financial decision making, *Natural Hazards*
643 *Observer*, Vol. XL, No. 7, October 2016, Natural Hazards Center, University of Colorado, Boulder, [Available at
644 <https://hazards.colorado.edu/article/money-matters-rapid-post-earthquake-financial-decision-making>], 2016.
645
- 646 Wald, D.J., and Franco, G.: Financial decision-making based on near-real-time earthquake information, in 16th
647 World Conference on Earthquake Engineering, Santiago, Chile, Jan 9th to 11th, 2017, paper #3625, 2017.
648
- 649 Wilson, T.M., Stewart, C., Sword-Daniels, V., Leonard, G.S., Johnston, D.M., Cole, J.W., Wardman, J., Wilson, G.,
650 and Barnard, S.T.: Volcanic ash impacts on critical infrastructure. *Physics and Chemistry of the Earth, Parts A/B/C*,
651 45, 5-23, doi: 10.1016/j.pce.2011.06.006, 2012-b.
652
- 653 World Economic Forum: Convergence of Insurance and Capital Markets. REF: 091008, World Economic Forum,
654 [Available at <https://www.weforum.org/reports/convergence-insurance-and-capital-markets>], 2008.
655
- 656 Yamamoto, T. and Nakada, S.: Extreme Volcanic Risks 2: Mount Fuji. In: *Volcanic Hazards, Risks and Disasters*.
657 Editor(s): John F. Shroder, Paolo Papale, Elsevier, doi: 10.1016/B978-0-12-396453-3.00014-9, 2015.
658
- 659 Yamasato, H., Funasaki, J. and Takagi, Y.: The Japan Meteorological Agency's Volcanic Disaster Mitigation
660 Initiatives. Technical Note of the NIED (National Research Institute for Earth Science and Disaster Prevention), No.
661 380, 101-107, 2013.
662
663
664
665
666
667
668
669
670
671
672
673
674
675
676
677
678
679
680



681 **Tables**

682

683

Volcano Name	Number of ash fall events	Aggregate Annual Occurrence Probability
Fuji	9,969	4.84×10^{-3}
Hakone	12,821	6.58×10^{-4}
Asama	832	8.45×10^{-5}
Haruna	651	3.95×10^{-5}
Kita-Yatsugatake	2,065	2.57×10^{-6}
Kusatsu-Shirane	469	6.01×10^{-6}

684

685 **Table 1: Number of volcanic ash fall events included in the model (i.e. those ash fall events that impact the model's**
 686 **geographical domain of Tokyo and Kanagawa prefectures) and associated annual probabilities of occurrence by volcano.**
 687 **Ash fall events originated by these volcanoes that do not impact the model domain have been excluded from the counts.**

688

689

690

691

692

693

694

695

696

697

698

699

700

701

702

703

704

705

706

707

708



709

Function ID	Occupancy	Construction Type	Building Rise	Roof Pitch
1	Resid., Comm. or Indust. Buildings	Wood Frame	Low	Medium
2	Resid., Comm. or Indust. Buildings	Wood Frame	Low	High
3	Resid., Comm. or Indust. Buildings	Wood Frame	Medium	Medium
4	Resid., Comm. or Indust. Buildings	Wood Frame	Medium	High
5	Resid., Comm. or Indust. Buildings	RC-SRC or Steel Frame	Low	Low-Medium
6	Resid., Comm. or Indust. Buildings	RC-SRC or Steel Frame	Low	High
7	Resid., Comm. or Indust. Buildings	RC-SRC or Steel Frame	Medium	Low-Medium
8	Resid., Comm. or Indust. Buildings	RC-SRC or Steel Frame	Medium	High
9	Resid., Comm. or Indust. Buildings	RC-SRC or Steel Frame	High	Low-Medium or High
10	Resid. Buildings	Light Metal Frame	Low	Medium
11	Resid. Buildings	Light Metal Frame	Low	High
12	Resid., Comm. or Indust. Buildings	Light Metal Frame	Medium	Medium
13	Resid., Comm. or Indust. Buildings	Light Metal Frame	Medium	High
14	Resid., Comm. or Indust. Buildings	Light Metal Frame	High	Medium
15	Resid., Comm. or Indust. Buildings	Light Metal Frame	High	High
16	Comm. or Indust. Buildings	Steel Frame or Light Metal Frame	Low	Low-Medium; long-span

710

711 **Table 2: Building types common in the Tokyo and Kanagawa Prefectures of Japan, for which specific vulnerability**
 712 **functions were developed in the volcano risk model. RC-SRC stands by “Reinforced Concrete – Steel Reinforced**
 713 **Concrete”.**

714
 715
 716
 717
 718
 719
 720
 721
 722
 723
 724
 725
 726
 727
 728
 729
 730
 731
 732
 733
 734
 735
 736
 737
 738



739

Prefecture	Type of Residential Dwelling	Representative reconstruction values (Million JPY)
Tokyo	Single Family	25.5
	Condominium	16.3
Kanagawa	Single Family	22.1
	Condominium	12.3

740

741 **Table 3: Representative reconstruction values have been estimated on the basis of several sources of information,**
742 **including data on building construction values from Japanese Government Statistics (<https://www.e-stat.go.jp>) and**
743 **insured building values from the General Insurance Rating Organization of Japan (<https://www.giroj.or.jp>).**

744

745

746

747

748

749

750

751

752

753

754

755

756

757

758

759

760

761

762

763

764

765

766



767

	Number of dwellings	Total Value (Million JPY)
Tokyo	6,435,994	121,605,115
Kanagawa	3,828,279	62,788,449
TOTAL	10,264,273	184,393,564

768

769 **Table 4: Total number of dwellings and total reconstruction values modelled in the volcano risk model for six Japanese**
770 **volcanoes (by prefecture, and totals). Number of dwellings from Japanese Government Statistics ([https://www.e-](https://www.e-stat.go.jp)**
771 **stat.go.jp); Total Values have been calculated on the basis of representative reconstruction values in Table 3.**

772

773

774

775

776

777

778

779

780

781

782

783

784

785

786

787

788

789

790

791

792

793

794

795

796

797

798

799

800

801

802

803

804

805

806

807

808

809

810

811

812

813

814

815



EventID	Volcano	Annual Event Rate	Mean Loss (JPY)	Loss S. Dev. (JPY) (Independent)	Loss S. Dev. (JPY) (Correlated)
1588	Fuji	9.84×10^{-8}	1.03×10^{12}	1.28×10^9	1.32×10^{11}
1589	Fuji	3.65×10^{-7}	1.87×10^6	2.25×10^6	1.93×10^7
1590	Fuji	4.91×10^{-8}	1.36×10^{13}	4.29×10^9	1.01×10^{12}
1591	Fuji	9.82×10^{-7}	0	0	0

816

817 **Table 5: Subset of ELT outputs from the volcano risk model, run of the residential portfolio described. The table shows**
 818 **losses on the portfolio caused by four of the model's ash fall events from Mt. Fuji. The mean loss and the standard**
 819 **deviation of the loss distribution associated to each event (in JPY) are reported in the ELT.**

820
 821
 822
 823
 824
 825
 826
 827
 828
 829
 830
 831
 832
 833
 834
 835
 836
 837
 838
 839
 840
 841
 842
 843
 844
 845
 846
 847
 848
 849
 850
 851
 852
 853
 854
 855
 856
 857
 858
 859
 860
 861
 862
 863



864
 865
 866

	Plume Height Thresholds [Km]								Yearly Exceedance Probability	Transferred Risk	Layer Payment
	N	NE	E	SE	S	SW	W	NW			
Layer 1	32	28	28	32	36	37	40	36	0.026%	76%	33%
Layer 2	33	32	29	33	37	40	41	37	0.020%	67%	100%

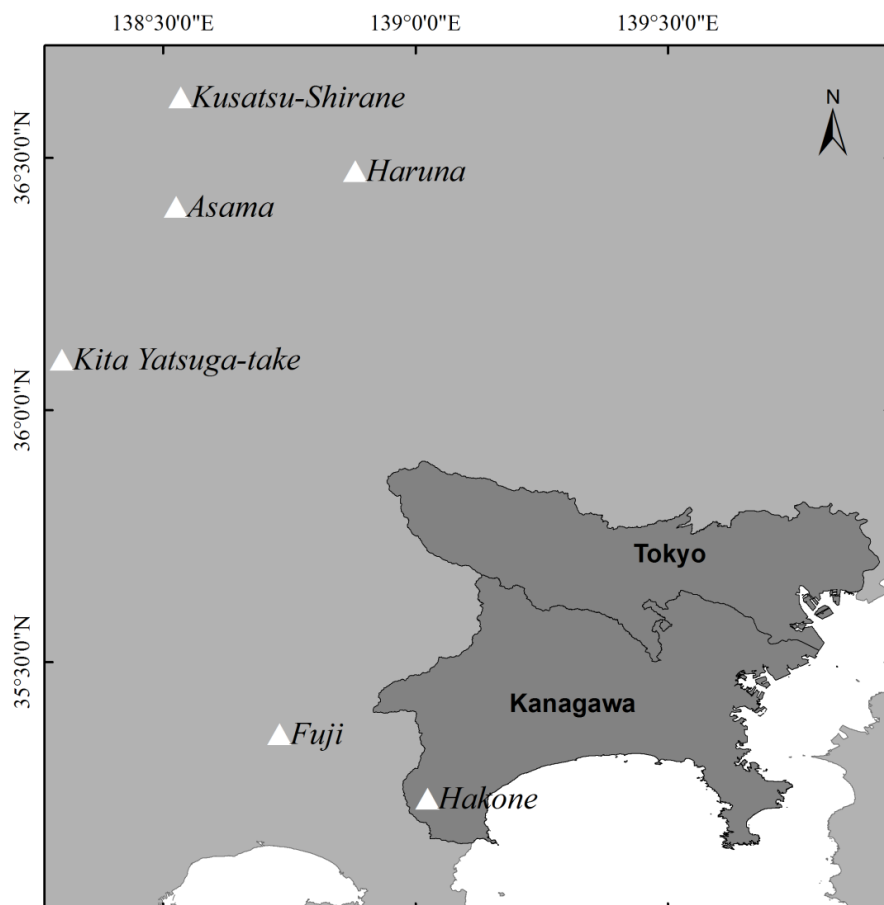
867

868 **Table 6: Parametric trigger for Mt Fuji. The risk transferred by each layer is expressed as percentage over the total risk**
 869 **of Mt Fuji. The layer payment is expressed as fraction of the maximum payment (300 Billion JPY).**

870
 871
 872
 873
 874
 875
 876
 877
 878
 879
 880
 881
 882
 883
 884
 885
 886
 887
 888
 889
 890
 891
 892
 893
 894
 895
 896
 897
 898
 899
 900
 901
 902
 903
 904
 905
 906
 907
 908
 909

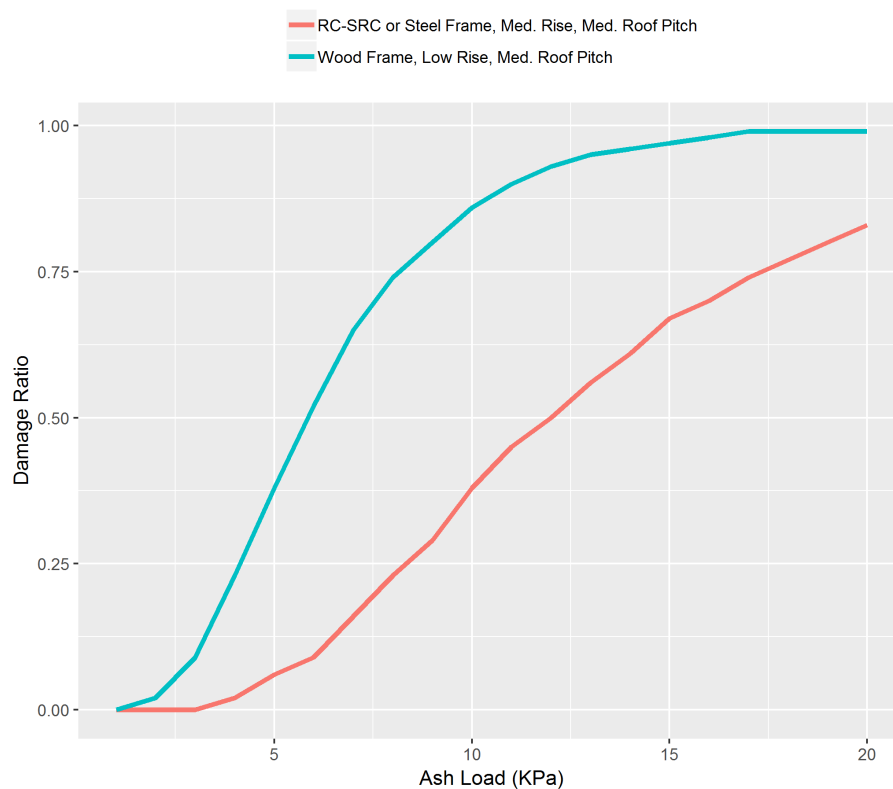


910 **Figures**
911
912
913



914
915 **Figure 1:** The geographic domain of the volcano ash fall model presented in this paper includes Tokyo and Kanagawa
916 Prefectures in Japan, and the six major volcanoes that can affect them, Fuji, Hakone, Asama, Haruna, Kita-Yatsugatake,
917 and Kusatsu-Shirane.

918
919
920
921
922
923
924
925
926
927



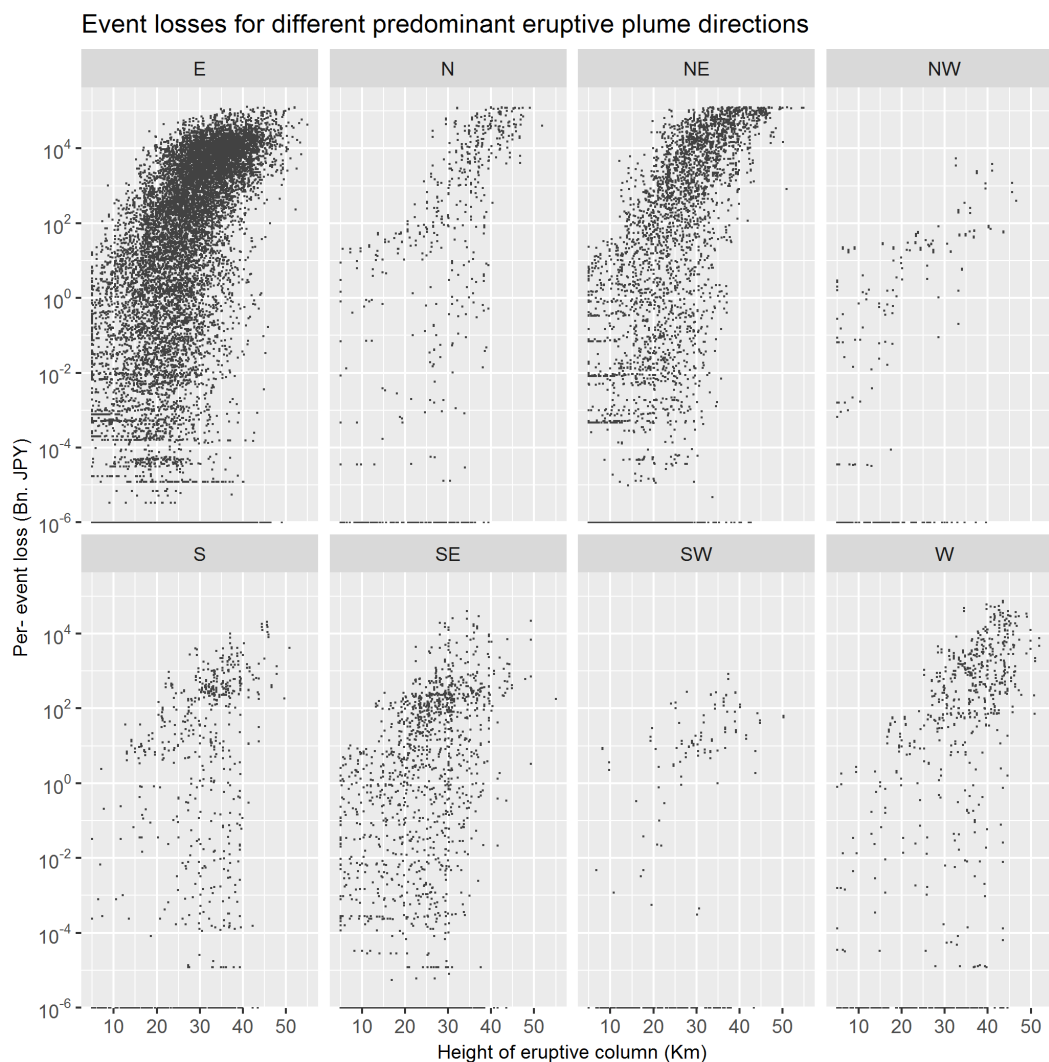
928
929
930
931
932
933

Figure 2: Damage functions for two different building types considered in the volcano risk model (“RC-SRC” stands for Reinforced Concrete- Steel Reinforced Concrete; “Med.” stands for Medium); source of these damage functions is Maqsood et al., 2014.

934
935
936
937
938
939
940
941
942
943
944
945
946
947
948
949
950
951
952



953
954
955
956



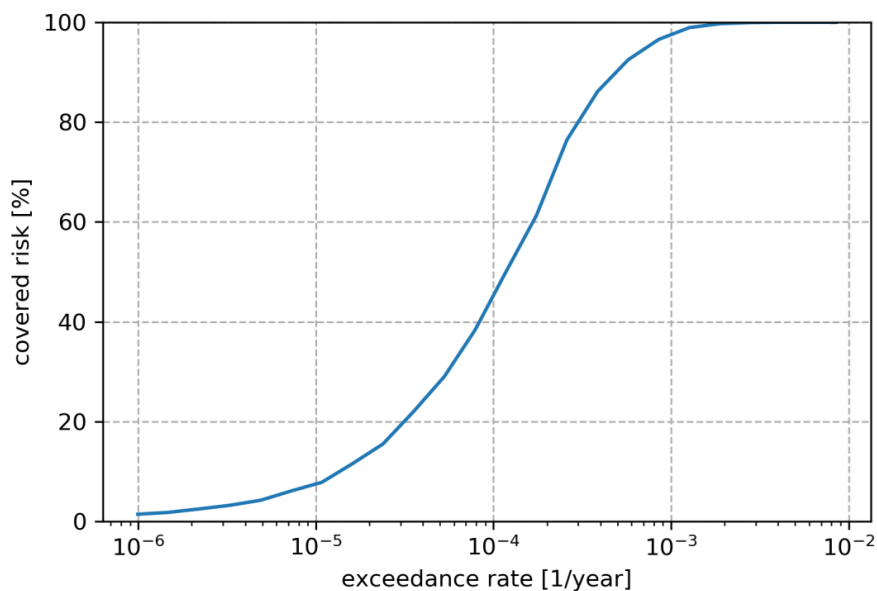
957

958 **Figure 3: Relationship between height of eruptive column (in Km, from crater rim) and modelled losses for all eruptive**
959 **events in the volcano risk model. Each panel displays a subset of eruptions featuring a specific predominant direction of**
960 **their eruptive plume (East, North, North-East, North-West, South, South-East, South-West and West).**

961
962
963
964
965
966



967
968



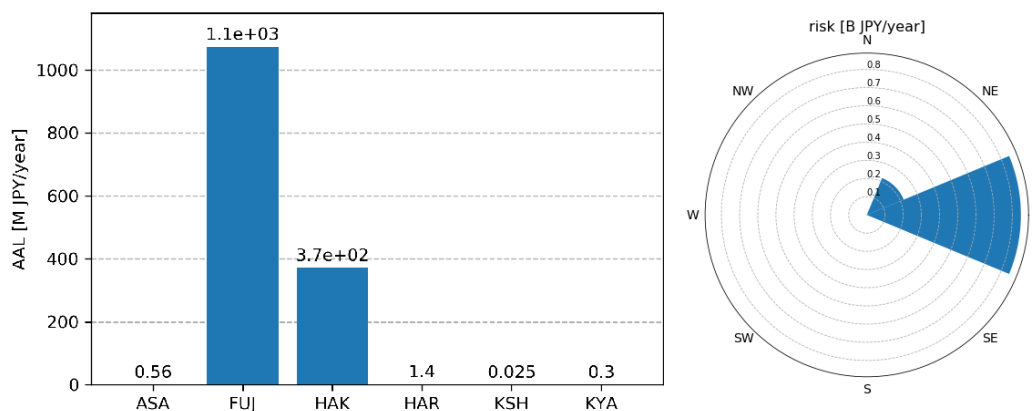
969
970
971
972

973 **Figure 4: Pareto front for a binary trigger designed modelling stochastic losses for Mt. Fuji. The transferred risk is**
974 **displayed as percentage of the total risk.**

975
976
977
978
979
980
981
982
983
984
985
986
987
988
989
990
991
992
993
994
995
996



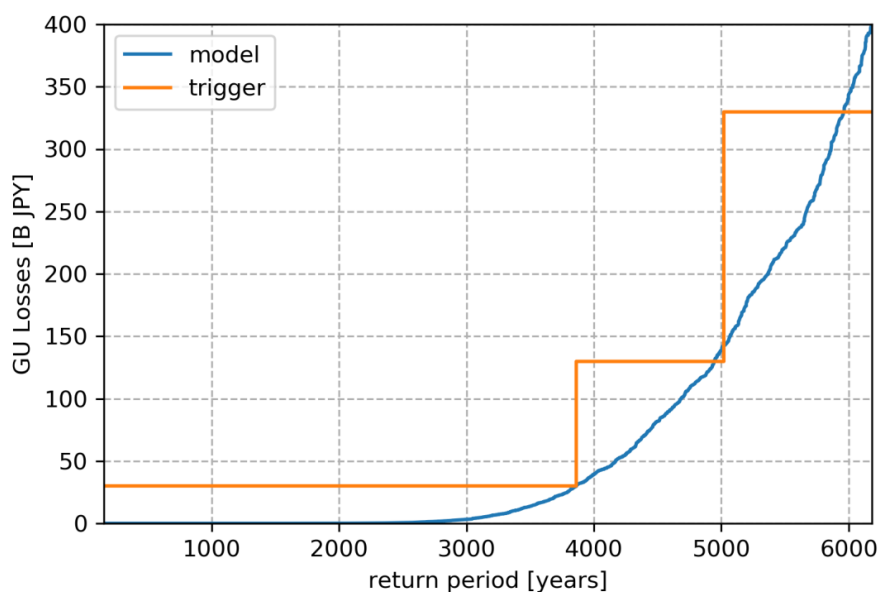
997
998
999



1000
1001
1002
1003
1004
1005

Figure 5: (Left) Modelled AAL for the six volcanoes included in the volcano risk model. (Right) Breakdown of Mt Fuji risk by wind sector.

1006
1007
1008
1009
1010
1011
1012
1013
1014
1015
1016
1017
1018
1019
1020
1021
1022
1023
1024
1025
1026
1027
1028
1029
1030
1031
1032
1033



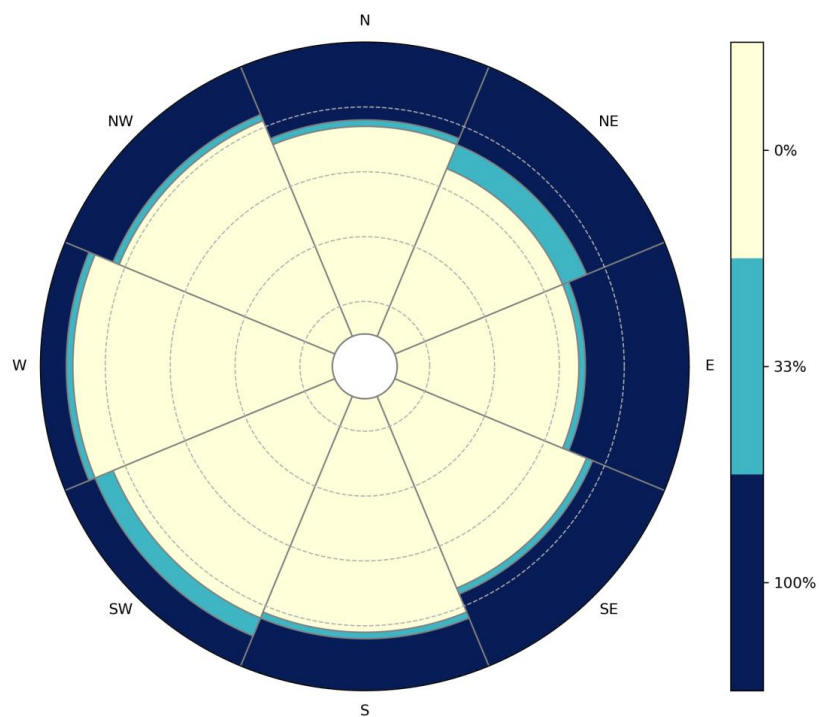
1034
1035
1036
1037

Figure 6: OEP curve for Mt Fuji losses (blue) and trigger payments (orange)

1038
1039
1040
1041
1042
1043
1044
1045
1046
1047
1048
1049
1050
1051
1052
1053
1054
1055
1056
1057
1058
1059
1060
1061
1062
1063
1064



1065



1066

1067 **Figure 7: Parametric Trigger for Mt. Fuji Each dashed line correspond to a unit of 10Km**

1068
1069
1070
1071
1072
1073
1074
1075
1076
1077
1078
1079
1080
1081
1082
1083
1084
1085
1086



1087

1088

1089 **Author contribution:**

1090

1091 Delioma Oramas-Dorta built the volcano risk model, produced the risk results (“ELT”) associated to the portfolio of
1092 residential properties used in the Application, and researched and defined the physical trigger parameters for the
1093 design of the volcano risk transfer mechanism presented in the paper. Giulio Tirabassi contributed to the definition
1094 of the physical trigger parameters, and coded the mathematical design and optimization of the trigger. Guillermo E.
1095 Franco developed the original code as applied to earthquakes, and oversaw the adaptation of the code to the case of
1096 volcanic eruptions. Christina Magill produced the tephra fall footprints used in the hazard module of the volcano
1097 risk model, while working at Risk Frontiers.

1098

1099

1100 **Acknowledgements:**

1101

1102 We would like thanking Guy Carpenter for permitting the use of its proprietary Volcano Risk Model for Six
1103 Volcanoes in Japan, in order to produce the risk/ loss estimates this study used as a basis to design a parametric risk
1104 transfer solution for volcanic eruptions. We would like to acknowledge the providers of several datasets that form
1105 part of this Volcano Risk Model. In particular, Risk Frontiers (<https://riskfrontiers.com/>) provided the set of
1106 stochastic volcanic tephra fall footprints that are part of the volcano risk model’s hazard module. These footprints
1107 were produced in 2017 following commission from Guy Carpenter, to form part of its proprietary Volcano Risk
1108 Model for Six Volcanoes in Japan. Development of volcanic tephra fall footprints by Risk Frontiers used wind
1109 reanalysis data (NCEP-DOE Reanalysis 2) from NOAA/OAR/ESRL PSD, Boulder, Colorado, USA
1110 (<https://www.esrl.noaa.gov/psd/>). Rainfall data that also form part of the model’s hazard module were provided by
1111 JBA Risk Management, www.jbarisk.com.

1112

1113

1114

1115